Cylinder gratings in conical incidence with applications to woodpile structures

G. H. Smith,[1] L. C. Botten,[1] R. C. McPhedran,[2] and N. A. Nicorovici[2]
[1]*CUDOS ARC Centre of Excellence and Department of Mathematical Sciences, University of Technology, Sydney, New South Wales 2007, Australia*
[2]*CUDOS ARC Centre of Excellence and School of Physics, University of Sydney, New South Wales 2006, Australia*
(Received 13 February 2003; published 21 May 2003)

We use our previous formulation for cylinder gratings in conical incidence to discuss the photonic band gap properties of woodpile structures. We study scattering matrices and Bloch modes of the woodpile, and use these to investigate the dependence of the optical properties on the number of layers. We give data on reflectance, transmittance and absorptance of metallic woodpiles as a function of wavelength and number of layers, using both the measured optical constants of tungsten and using a perfect conductivity idealization to characterize the metal. For semi-infinite metallic woodpiles, we show that polarization of the incident field is important, highlighting the role played by surface effects as opposed to lattice effects.

DOI: 10.1103/PhysRevE.67.056620 PACS number(s): 42.25.Fx, 42.70.Qs, 42.81.Dp, 78.20.Bh

I. INTRODUCTION

In our previous paper [1], we developed a formulation for stacked parallel gratings in conical incidence, using a multipole method. In this paper, we apply the theory to the analysis of the woodpile photonic crystal. This is a structure consisting of layers of cylindrical rods with a stacking sequence that repeats itself every four layers. Within each layer, the rods are parallel and separated by a distance D. The distance between successive layer centers is h and the rod axes in adjacent layers are orthogonal. To obtain a periodicity of four layers in the stacking direction, rods separated by one intermediate layer are offset by a distance of $D/2$ in the direction perpendicular to the rod axes (Fig. 1). A list of references relating to the origin of the woodpile geometry may be found in the web bibliography of Dowling, Everitt, and Yablonovitch [2]. Early theoretical studies of the woodpile were made by Ho *et al.* [3], using layers of dielectric rods of circular, elliptical, or rectangular shape, by Özbay *et al.* [4] and by Sözüer and Dowling [5].

The woodpile has attracted much attention since it is a three-dimensional structure, yet it can be fabricated using two-dimensional lithography in a multistep process. At Sandia Laboratories, Lin and Fleming [6,7] have fabricated a structure exhibiting a band gap at the important telecommunications wavelength band near 1.5 μm. Similar crystals have been constructed by Noda *et al.* [8].

Recently, metallic woodpile structures have been investigated by Lin *et al.* [9] and El-Kady *et al.* [10]. Metallic photonic crystals with a microstructure based on spheres, with the Drude model used for the metal, are also discussed by Modinos *et al.* [11]. Metallic crystals offer advantages in size and weight, they are easier to fabricate and the costs are lower. There are potentially high temperature applications in thermophotovoltaics and blackbody emission. The crystal manufactured by Lin *et al.* [9] has a large band gap in the infrared region (8 μm to >20 μm), together with an absorption peak near the band edge. A potential application of this effect is an efficient incandescent lamp in which energy radiation could be suppressed in the infrared and shifted into the visible region.

The woodpile structure we study here is an assemblage of circular cylinders, which may be composed of either dielectric or metal. The ability to treat metallic gratings, including perfectly conducting gratings, is a strong feature of our method. For simplicity, we will consider the case where the unit cell of the grating contains only one cylinder, although the generalization to multiple cylinders per unit cell is straightforward and valuable [12]. A solution of the problem in terms of a single scalar potential (cf. Ref. [13]) is not possible due to the crossed structure of successive gratings and the polarization coupling that occurs through the boundary conditions. The prescription of the scattering matrix requires the solution of a family of conical incidence diffraction problems for each layer associated with the dispersion directions introduced by the previous layer.

We note that Li [14] has treated conical diffraction by gratings composed of rectangular rods, generalizing our earlier work on a modal formulation for dielectric and metallic lamellar gratings [15], while Centeno and Felbacq [16,17] consider the behavior of band gaps in photonic crystals as functions of polarization and conicity of the incident plane wave. Li's formulation has been exploited in a recent work on woodpiles composed of dielectric lamellar gratings in the thesis by Gralak [18]. Woodpile crystals and, in particular, dispersion relations and band gaps in dielectric woodpiles,

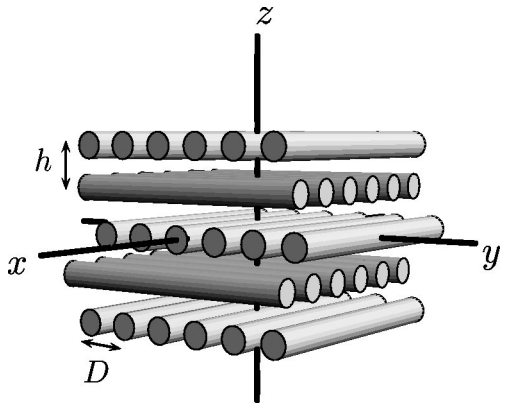

FIG. 1. The woodpile structure.

were further discussed by Gralak *et al.* [19].

In Sec. II, we establish notation and summarize our formulation for gratings in conical incidence. In Sec. III, we develop the formulation for the specific case of the woodpile structure. In Sec. IV, we discuss Bloch modes of the woodpile and derive an algorithm that quantifies the dependence of the transmittance, reflectance, and absorptance on the number of layers. This is an important information for those involved in the fabrication of such structures. Finally in Sec. V, we study the reflectance, transmittance, and absorptance for tungsten woodpiles and relate these to the theoretical considerations in Sec. IV, while showing the importance of surface effects not evident in the Bloch analysis.

II. CONICAL DIFFRACTION THEORY

In this section, we establish notation and give a self-contained summary of the essential features of our formulation for cylinder gratings in conical incidence, using a Rayleigh multipole method [12,20]. Full details are given in Ref. [1]. A major advantage of the multipole method lies in its ability to treat metallic and dielectric gratings with equal ease. Our calculations for metallic woodpiles use measured values of optical constants, such as those found in Ref. [21]. For comparison purposes, we shall also use an idealized (perfect conductivity) model.

We consider a single grating consisting of identical parallel cylindrical rods of radius a whose axes are separated by a distance D. In the chosen Cartesian coordinate system, the cylinders are parallel to the x-y plane with their axes parallel to the x axis, as in the middle layer of Fig. 1. The primary incidence channel is defined by the wave vector

$$\mathbf{k}_i=(\alpha_0,\beta_0,-\gamma_0), \tag{1}$$

with wavenumber $k=\omega/c=(\alpha_0^2+\beta_0^2+\gamma_0^2)^{1/2}$, where ω is the angular frequency and c is the speed of light in vacuum.

The periodicity of the layer of cylinders introduces dispersion in the y direction characterized by $e^{i\beta_q y}$, with $\beta_q=\beta_0+2\pi q/D$. For in-plane incidence in either of the two principal polarizations, the problem is x invariant for a single layer. However, in conical diffraction, the x dependence is $e^{i\alpha_0 x}$ while the addition of an orthogonal layer, as in a woodpile, introduces dispersion in the x direction, leading to an x dependence of $e^{i\alpha_p x}$, with $\alpha_p=\alpha_0+2\pi p/D$. The formulation of the single layer scattering matrices for a 2D diffraction problem in such configurations thus requires the solution of the family $\{p\}$ of diffraction problems, each one associated with a particular α_p direction. For convenience, we index plane wave coefficients by $s=(p,q)\in\mathbb{Z}^2$. Putting $\mathbf{Q}_s=\alpha_p\hat{\mathbf{x}}+\beta_q\hat{\mathbf{y}}$, we can write the z dependence of plane wave fields as $e^{\pm i\gamma_s z}$, where

$$\gamma_s=\sqrt{k^2-Q_s^2},\quad s\in\Omega_r=\{s|Q_s^2\leqslant k^2\}, \tag{2}$$

$$\gamma_s=i\sqrt{Q_s^2-k^2},\quad s\in\Omega_e=\{s|Q_s^2>k^2\}. \tag{3}$$

Let us begin by restricting ourselves to conical diffraction of fields with a specified x dependence of $e^{i\alpha_p x}$.

Field quantities are expressed in terms of the TE and TM components of the electric field with respect to the vertical z axis. In the half space above the grating, $\mathbf{E}_I^-=[E_{I,s}^-]$ and $\mathbf{F}_I^-=[F_{I,s}^-]$, respectively, denote the TE and TM components of the incoming electric field, indexed by the channel number $s=(p,q)$. Similarly, $\mathbf{E}_D^+=[E_{D,s}^+]$ and $\mathbf{F}_D^+=[F_{D,s}^+]$, respectively, denote the TE and TM components of the outgoing electric field. In the half space below the grating, $\mathbf{E}_I^+$ and $\mathbf{F}_I^+$ denote the TE and TM components of the incoming electric field and $\mathbf{E}_D^-$ and $\mathbf{F}_D^-$ denote the TE and TM components of the outgoing electric field. These TE and TM components are combined as block matrices according to

$$\boldsymbol{\mathcal{F}}_D^{\pm}=\begin{bmatrix}\mathbf{E}_D^{\pm}\\ \mathbf{F}_D^{\pm}\end{bmatrix},\quad \boldsymbol{\mathcal{F}}_I^{\pm}=\begin{bmatrix}\mathbf{E}_I^{\pm}\\ \mathbf{F}_I^{\pm}\end{bmatrix}. \tag{4}$$

Where necessary, we shall indicate x dependence of the form $e^{i\alpha_p x}$ by a subscript [as in $\boldsymbol{\mathcal{F}}_{I,\alpha_p}^{\pm}$] or by parentheses [as in $\mathsf{S}(\alpha_p)$]. The scattering matrix relates the outgoing fields to the incident fields and, with a minor change of notation, we show in Ref. [1] that

$$\begin{bmatrix}\boldsymbol{\mathcal{F}}_D^-\\ \boldsymbol{\mathcal{F}}_D^+\end{bmatrix}=\mathsf{S}\begin{bmatrix}\boldsymbol{\mathcal{F}}_I^-\\ \boldsymbol{\mathcal{F}}_I^+\end{bmatrix}, \tag{5}$$

where the matrix $\mathsf{S}=\mathsf{S}(\alpha_p)$ has the form

$$\mathsf{S}=\mathsf{T}^{-1}\left(\mathsf{I}-\frac{k}{k_\perp^2 D}\mathsf{X}\begin{bmatrix}\boldsymbol{\mathcal{K}}^s\boldsymbol{\mathcal{L}}\boldsymbol{\mathcal{J}}^s & \boldsymbol{\mathcal{K}}^s\boldsymbol{\mathcal{L}}\boldsymbol{\mathcal{J}}^a\\ \boldsymbol{\mathcal{K}}^a\boldsymbol{\mathcal{L}}\boldsymbol{\mathcal{J}}^s & \boldsymbol{\mathcal{K}}^a\boldsymbol{\mathcal{L}}\boldsymbol{\mathcal{J}}^a\end{bmatrix}\mathsf{X}\right)\mathsf{T}. \tag{6}$$

In Eq. (6), the identity matrix represents the scattering operator in the absence of the grating, while the second term represents the diffracted field. A short explanation of the various terms occurring in this equation follows; for a full discussion, we refer to Ref. [1]. In Eq. (6), $k_\perp^2=k^2-\alpha_p^2$ and T is the transformation

$$\mathsf{T}=\begin{bmatrix}\boldsymbol{\mathcal{I}} & \boldsymbol{\mathcal{I}}\\ \boldsymbol{\mathcal{I}} & -\boldsymbol{\mathcal{I}}\end{bmatrix}, \tag{7}$$

which reflects the symmetry relationships between electric and magnetic quantities that are imposed by Maxwell's equations. The matrices $\boldsymbol{\mathcal{I}}$ or I denote the identity matrix of appropriate size. The matrix

$$\boldsymbol{\mathcal{L}}=(\boldsymbol{\mathcal{M}}+\boldsymbol{\mathcal{S}})^{-1} \tag{8}$$

is the scattering operator in a cylindrical harmonic basis and incorporates the lattice geometry within the Toeplitz matrix $\boldsymbol{\mathcal{S}}$ of lattice sums [22,23] and the material properties of the structure (refractive indices and radii) within the matrix $\boldsymbol{\mathcal{M}}$. This separation of the lattice geometry and the material properties of the structure is an analytically and computationally attractive feature that is common to all Rayleigh multipole methods. The matrices $\boldsymbol{\mathcal{J}}^a$ and $\boldsymbol{\mathcal{J}}^s$ reflect a change of basis from plane waves into cylindrical harmonics, and $\boldsymbol{\mathcal{K}}^a$ and $\boldsymbol{\mathcal{K}}^s$ represent the inverse transformation. The indices a and s refer to a generalization of the symmetric and antisymmetric

problems discussed in Ref. [13]. While the plane wave diffraction problem is best formulated in terms of TE and TM modes, the multipole scattering problem, as developed in Ref. [1], is best handled in terms of principal Cartesian field components parallel to the cylinder axes. These two representations are related by the matrix X.

Equation (6) makes no assumptions about the physical symmetry of the scattering elements of the grating. However, as shown in Ref. [1], the terms $\mathcal{K}^s\mathcal{L}\mathcal{J}^a$ and $\mathcal{K}^a\mathcal{L}\mathcal{J}^s$ vanish for gratings having an up-down symmetry, in which case the system decouples completely into a symmetric and an antisymmetric problem [13].

We can also derive terms for the reflection and transmission scattering matrices. Let $\mathcal{R}_a$ and $\mathcal{R}_b$, respectively, denote reflection scattering matrices for incidence above and below the grating and let $\mathcal{T}_a$ and $\mathcal{T}_b$ denote the corresponding transmission scattering matrices. Clearly the matrix S of Eq. (6) can be expressed in the form

$$\mathsf{S}=\begin{bmatrix} \mathcal{T}_a & \mathcal{R}_b \\ \mathcal{R}_a & \mathcal{T}_b \end{bmatrix}, \tag{9}$$

so that

$$\begin{bmatrix} \mathcal{F}_D^- \\ \mathcal{F}_D^+ \end{bmatrix}=\begin{bmatrix} \mathcal{T}_a & \mathcal{R}_b \\ \mathcal{R}_a & \mathcal{T}_b \end{bmatrix}\begin{bmatrix} \mathcal{F}_I^- \\ \mathcal{F}_I^+ \end{bmatrix}. \tag{10}$$

A comparison between Eqs. (5) and (10) thus yields explicit expressions for the transmission and reflection matrices. When the grating is up-down symmetric, we find [1,13]

$$\mathcal{R}_a=\mathcal{R}_b=-\frac{k}{2k_\perp^2 D}\mathcal{X}(\mathcal{K}^s\mathcal{L}\mathcal{J}^s-\mathcal{K}^a\mathcal{L}\mathcal{J}^a)\mathcal{X}, \tag{11}$$

$$\mathcal{T}_a=\mathcal{T}_b=\mathcal{I}-\frac{k}{2k_\perp^2 D}\mathcal{X}(\mathcal{K}^s\mathcal{L}\mathcal{J}^s+\mathcal{K}^a\mathcal{L}\mathcal{J}^a)\mathcal{X}. \tag{12}$$

We now consider the family $\{p\}$ of diffraction problems associated with all possible α_p directions. This is a two-dimensional-grid environment and we compute a family of 1D-grating scattering matrices each of which is associated with a direction α_p. We fill the 2D-grid matrix to get a scattering matrix $\tilde{\mathsf{S}}$ of the form

$$\tilde{\mathsf{S}}=\begin{bmatrix} \ddots & & & & \\ & \mathsf{S}(\alpha_{-1}) & 0 & 0 & \\ & 0 & \mathsf{S}(\alpha_0) & 0 & \\ & 0 & 0 & \mathsf{S}(\alpha_1) & \\ & & & & \ddots \end{bmatrix}. \tag{13}$$

In Eq. (13), it is assumed that $\tilde{\mathsf{S}}$ acts on incident fields that follow the natural order

$$\cdots \mathcal{F}^-_{I,\alpha_{-1}},\mathcal{F}^+_{I,\alpha_{-1}},\mathcal{F}^-_{I,\alpha_0},\mathcal{F}^+_{I,\alpha_0},\mathcal{F}^-_{I,\alpha_1},\mathcal{F}^+_{I,\alpha_1},\cdots. \tag{14}$$

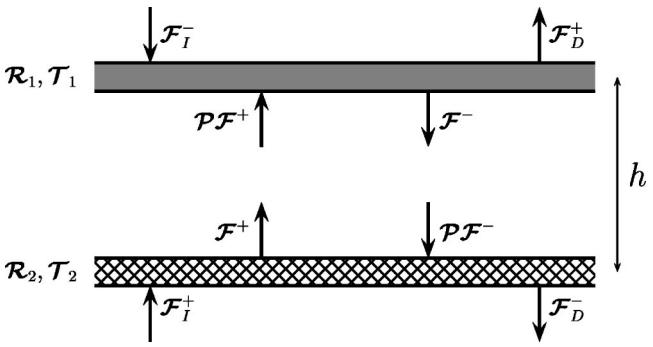

FIG. 2. A pair of up-down symmetric gratings.

In numerical implementations, we need to choose a minimum number of channels that ensures accuracy. As discussed in Sec. III, this entails truncation of the matrix $\tilde{\mathsf{S}}$ and permutation of the remaining entries, effectively changing the incident field order given above. Typically, 21 cylindrical harmonics are included in calculations, together with plane wave orders between -5 and 5 in both directions, and reflectance and transmittance results are accurate to six figures [1]. Absorptance results are deduced using conservation of energy for structures with loss, while for dielectric and perfectly conducting structures the conservation of energy is guaranteed by the structure of the formulation [24].

III. THE WOODPILE STRUCTURE

In order to obtain reflection and transmission scattering matrices for the woodpile structure, we first derive the scattering matrices for the basic unit, namely, a pair of crossed gratings. We then use a well-established algorithm [13] to form a stack of such crossed pairs.

A. Crossed cylinder gratings

As mentioned in Sec. II, the plane wave diffracted orders in a pair of crossed gratings are a doubly infinite set, indexed by pairs (p,q) corresponding to diffraction in the plane of each grating. Here, q enumerates the diffracted orders of the grating with generators parallel to the x axis, while p enumerates the orders of the orthogonal grating. For either grating, there is dispersion in only one direction and thus the 2D scattering matrix for a single grating is essentially a block diagonal matrix with each block being the scattering matrix for a 1D problem indexed over, say, channels q, and driven with incidence parameters corresponding to channel p of the orthogonal grating.

As a necessary preliminary, consider an arbitrary pair of up-down symmetric planar gratings, separated by a distance h. The incident field is $[(\mathcal{F}_I^-)^T(\mathcal{F}_I^+)^T]^T$, the diffracted field is $[(\mathcal{F}_D^-)^T(\mathcal{F}_D^+)^T]^T$, and the downgoing and upgoing fields between the grating pair are $\mathcal{F}^-$ and $\mathcal{F}^+$, respectively (Fig 2).

Let $\tilde{\mathcal{R}}_j$ and $\tilde{\mathcal{T}}_j$, $j=1,2$, respectively, denote reflection and transmission scattering matrices for the top $(j=1)$ and bottom $(j=2)$ up-down symmetric gratings. Since the phases of the plane waves are referenced with respect to the

center of each grating, an arbitrary plane wave propagating between the gratings experiences a shift in phase of $\exp(i\gamma_p h)$. The propagation of a plane wave field $\boldsymbol{\mathcal{F}}$ may thus be written as $\boldsymbol{\mathcal{P}}\boldsymbol{\mathcal{F}}$ where $\boldsymbol{\mathcal{P}}=\mathrm{diag}[\mathbf{P},\mathbf{P}]$ and $\mathbf{P}=\mathrm{diag}[\exp(i\gamma_p h)]$. We have

$$\boldsymbol{\mathcal{F}}^- = \tilde{\boldsymbol{\mathcal{T}}}_1 \boldsymbol{\mathcal{F}}_I^- + \tilde{\boldsymbol{\mathcal{R}}}_1 \boldsymbol{\mathcal{P}} \boldsymbol{\mathcal{F}}^+, \tag{15}$$

$$\boldsymbol{\mathcal{F}}^+ = \tilde{\boldsymbol{\mathcal{T}}}_2 \boldsymbol{\mathcal{F}}_I^+ + \tilde{\boldsymbol{\mathcal{R}}}_2 \boldsymbol{\mathcal{P}} \boldsymbol{\mathcal{F}}^-, \tag{16}$$

$$\boldsymbol{\mathcal{F}}_D^- = \tilde{\boldsymbol{\mathcal{T}}}_2 \boldsymbol{\mathcal{P}} \boldsymbol{\mathcal{F}}^- + \tilde{\boldsymbol{\mathcal{R}}}_2 \boldsymbol{\mathcal{F}}_I^+, \tag{17}$$

$$\boldsymbol{\mathcal{F}}_D^+ = \tilde{\boldsymbol{\mathcal{T}}}_1 \boldsymbol{\mathcal{P}} \boldsymbol{\mathcal{F}}^+ + \tilde{\boldsymbol{\mathcal{R}}}_1 \boldsymbol{\mathcal{F}}_I^-. \tag{18}$$

Elimination of $\boldsymbol{\mathcal{F}}^-$ and $\boldsymbol{\mathcal{F}}^+$ from Eqs. (15)–(18) yields

$$\begin{bmatrix} \boldsymbol{\mathcal{F}}_D^- \\ \boldsymbol{\mathcal{F}}_D^+ \end{bmatrix} = \begin{bmatrix} \tilde{\boldsymbol{\mathcal{T}}}_2 & 0 \\ 0 & \tilde{\boldsymbol{\mathcal{T}}}_1 \end{bmatrix} \begin{bmatrix} \tilde{\boldsymbol{\mathcal{P}}} & 0 \\ 0 & \tilde{\boldsymbol{\mathcal{P}}} \end{bmatrix} \begin{bmatrix} \boldsymbol{\mathcal{I}} & -\tilde{\boldsymbol{\mathcal{R}}}_1 \boldsymbol{\mathcal{P}} \\ -\tilde{\boldsymbol{\mathcal{R}}}_2 \boldsymbol{\mathcal{P}} & \boldsymbol{\mathcal{I}} \end{bmatrix}^{-1} \times \begin{bmatrix} \tilde{\boldsymbol{\mathcal{T}}}_1 & 0 \\ 0 & \tilde{\boldsymbol{\mathcal{T}}}_2 \end{bmatrix} \begin{bmatrix} \boldsymbol{\mathcal{F}}_I^- \\ \boldsymbol{\mathcal{F}}_I^+ \end{bmatrix} + \begin{bmatrix} 0 & \tilde{\boldsymbol{\mathcal{R}}}_2 \\ \tilde{\boldsymbol{\mathcal{R}}}_1 & 0 \end{bmatrix} \begin{bmatrix} \boldsymbol{\mathcal{F}}_I^- \\ \boldsymbol{\mathcal{F}}_I^+ \end{bmatrix}. \tag{19}$$

The matrix inversion in Eq. (19) may be performed using the easily checked matrix identity

$$\begin{bmatrix} \boldsymbol{\mathcal{I}} & \boldsymbol{\mathcal{A}} \\ \boldsymbol{\mathcal{B}} & \boldsymbol{\mathcal{I}} \end{bmatrix}^{-1} = \begin{bmatrix} (\boldsymbol{\mathcal{I}}-\boldsymbol{\mathcal{A}}\boldsymbol{\mathcal{B}})^{-1} & -\boldsymbol{\mathcal{A}}(\boldsymbol{\mathcal{I}}-\boldsymbol{\mathcal{B}}\boldsymbol{\mathcal{A}})^{-1} \\ -\boldsymbol{\mathcal{B}}(\boldsymbol{\mathcal{I}}-\boldsymbol{\mathcal{A}}\boldsymbol{\mathcal{B}})^{-1} & (\boldsymbol{\mathcal{I}}-\boldsymbol{\mathcal{B}}\boldsymbol{\mathcal{A}})^{-1} \end{bmatrix}. \tag{20}$$

Let $\boldsymbol{\mathcal{R}}_\nu^s$ and $\boldsymbol{\mathcal{T}}_\nu^s$ denote the reflection and transmission scattering matrices of the composite structure with $\nu=a$ denoting incidence from above and $\nu=b$ denoting incidence from below the structure. Then $\boldsymbol{\mathcal{R}}_a^s$, $\boldsymbol{\mathcal{T}}_a^s$, $\boldsymbol{\mathcal{R}}_b^s$, and $\boldsymbol{\mathcal{T}}_b^s$ satisfy an equation analogous to Eq. (10). Comparison of Eqs. (10) and (19), together with the use of Eq. (20), yields the results [13]

$$\boldsymbol{\mathcal{R}}_a^s = \tilde{\boldsymbol{\mathcal{R}}}_1 + \tilde{\boldsymbol{\mathcal{T}}}_1 \boldsymbol{\mathcal{P}} \tilde{\boldsymbol{\mathcal{R}}}_2 \boldsymbol{\mathcal{P}} (\boldsymbol{\mathcal{I}} - \tilde{\boldsymbol{\mathcal{R}}}_1 \boldsymbol{\mathcal{P}} \tilde{\boldsymbol{\mathcal{R}}}_2 \boldsymbol{\mathcal{P}})^{-1} \tilde{\boldsymbol{\mathcal{T}}}_1, \tag{21}$$

$$\boldsymbol{\mathcal{T}}_a^s = \tilde{\boldsymbol{\mathcal{T}}}_2 \boldsymbol{\mathcal{P}} (\boldsymbol{\mathcal{I}} - \tilde{\boldsymbol{\mathcal{R}}}_1 \boldsymbol{\mathcal{P}} \tilde{\boldsymbol{\mathcal{R}}}_2 \boldsymbol{\mathcal{P}})^{-1} \tilde{\boldsymbol{\mathcal{T}}}_1, \tag{22}$$

$$\boldsymbol{\mathcal{R}}_b^s = \tilde{\boldsymbol{\mathcal{R}}}_2 + \tilde{\boldsymbol{\mathcal{T}}}_2 \boldsymbol{\mathcal{P}} \boldsymbol{\mathcal{R}}_1 \boldsymbol{\mathcal{P}} (\boldsymbol{\mathcal{I}} - \tilde{\boldsymbol{\mathcal{R}}}_2 \boldsymbol{\mathcal{P}} \tilde{\boldsymbol{\mathcal{R}}}_1 \boldsymbol{\mathcal{P}})^{-1} \tilde{\boldsymbol{\mathcal{T}}}_2, \tag{23}$$

$$\boldsymbol{\mathcal{T}}_b^s = \tilde{\boldsymbol{\mathcal{T}}}_1 \boldsymbol{\mathcal{P}} (\boldsymbol{\mathcal{I}} - \tilde{\boldsymbol{\mathcal{R}}}_2 \boldsymbol{\mathcal{P}} \tilde{\boldsymbol{\mathcal{R}}}_1 \boldsymbol{\mathcal{P}})^{-1} \tilde{\boldsymbol{\mathcal{T}}}_2. \tag{24}$$

The basic woodpile unit is a crossed grating pair consisting of two layers of cylinders at right angles to each other. We take a primary system, denoted by xyz, in which the top grating is in the x-y plane and the cylinders in this layer are parallel to the x axis. We introduce a secondary coordinate system, denoted by $x'y'z'$, with $x'=y$, $y'=-x$, and $z'=z$. In this system, cylinders in the bottom layer are parallel to the x' axis. In what follows, primed quantities for the bottom grating are assumed to be taken with reference to $x'y'z'$, while unprimed quantities for the top grating are taken with reference to xyz.

The primary channel is $(\alpha_0,\beta_0,-\gamma_0)$. If the physical parameters (refractive index, diameter and position of the cylinders) of the grating are fixed, then the matrix $\tilde{\mathsf{S}}$ in Eq. (13) depends only on ω and $\mathbf{k}_i$:

$$\tilde{\mathsf{S}} = \tilde{\mathsf{S}}(\omega, \mathbf{k}_i). \tag{25}$$

In the xyz system, the wave vector $\mathbf{k}_i$ has the representation $\alpha_0\hat{\mathbf{x}}+\beta_0\hat{\mathbf{y}}-\gamma_0\hat{\mathbf{z}}$, while in the $x'y'z'$ system it has the representation $\alpha_0'\hat{\mathbf{x}}'+\beta_0'\hat{\mathbf{y}}'-\gamma_0'\hat{\mathbf{z}}'$, where

$$\alpha_0' = \beta_0, \quad \beta_0' = -\alpha_0, \quad \gamma_{00}' = \gamma_{00}. \tag{26}$$

It follows that

$$\alpha_p' = \beta_0 + \frac{2p\pi}{d} = \beta_p,$$

$$\beta_q' = -\alpha_0 + \frac{2q\pi}{d} = -\alpha_{-q},$$

$$\gamma_{pq}' = \gamma_{-q,p}. \tag{27}$$

These equations allow us to obtain the scattering matrix for the bottom grating, expressed in terms of $x'y'z'$. This is done by formal replacement of α_p by α_p', β_q by β_q', and γ_{pq} by γ_{pq}' in expression (25) for $\tilde{\mathsf{S}}$. The expressions for the top and bottom scattering matrices assume the natural channel order (14) in their respective coordinate systems. However, these orderings are physically different in that channels (p,q) and $(p,q)'$ represent different plane waves in general. From equations (27), we see that the wave vector $\alpha_p'\hat{\mathbf{x}}'+\beta_q'\hat{\mathbf{y}}'\pm\gamma_{pq}'\hat{\mathbf{z}}'$, representing channel $(p,q)'$, is identical to the wave vector $\alpha_{-q}\hat{\mathbf{x}}+\beta_p\hat{\mathbf{y}}\pm\gamma_{-q,p}\hat{\mathbf{z}}$, representing channel $(-q,p)$, so that channels $(p,q)'$ and $(-q,p)$ are physically identical. Similarly, channels (p,q) and $(q,-p)'$ are identical. Consequently, if we wish to use the same channel order in both the scattering matrices, it is necessary to appropriately reorder the entries in one (or both) of these scattering matrices.

For computational purposes, we order the channels $\{(p,q)\}$ by the values of γ_{pq}^2 and then restrict ourselves to a finite subset of $\{\gamma_{pq}^2 : -\infty<p,q<\infty\}$, namely, those values of γ_{pq}^2 which correspond to propagating orders ($\gamma_{pq}^2>0$), as well as enough evanescent orders ($\gamma_{pq}^2<0$) to ensure the required convergence. We thus have a definite order of channels $(p_1,q_1),\ldots,(p_n,q_n)$ and our reordering of matrix elements must change the order of the entries for the top and bottom scattering matrices to ensure that this order is the input and output order for both of them.

We can use these scattering matrices and Eqs. (21)–(24) to obtain reflection and transmission matrices for the pair of crossed gratings.

B. Grating stacks

Using a pair of crossed gratings as our basic structure, we can form a stack of such gratings, using a procedure similar

to that given in Ref. [13]. Equations (21)–(24) refer to phase origins on the horizontal plane of symmetry of each grating. We shall denote reflection and transmission matrices referred to these phase origins by a superscripted zero. In forming stacks of such pairs, it is advantageous to incorporate into the reflection and transmission matrices both the matrix $\mathcal{P}$, describing the propagation between layers, and the matrix $\mathcal{Q}$, describing the horizontal shift between successive pairs. This has the effect of encapsulating each grating pair in a symmetric layer of total thickness h. We find [1,25]

$$\begin{bmatrix} \mathcal{T}_a & \mathcal{R}_b \\ \mathcal{R}_a & \mathcal{T}_b \end{bmatrix} = \mathsf{QP} \begin{bmatrix} \mathcal{T}_a^{(0)} & \mathcal{R}_b^{(0)} \\ \mathcal{R}_a^{(0)} & \mathcal{T}_b^{(0)} \end{bmatrix} \mathsf{PQ}, \tag{28}$$

where

$$\mathsf{Q} = \begin{bmatrix} \mathcal{Q}^{-1/2} & \mathbf{0} \\ \mathbf{0} & \mathcal{Q}^{1/2} \end{bmatrix}, \quad \mathsf{P} = \begin{bmatrix} \mathcal{P}^{1/2} & \mathbf{0} \\ \mathbf{0} & \mathcal{P}^{1/2} \end{bmatrix}, \tag{29}$$

$$\mathcal{Q} = \mathrm{diag}[\mathbf{Q}, \mathbf{Q}], \quad \mathcal{P} = \mathrm{diag}[\mathbf{P}, \mathbf{P}], \tag{30}$$

$$\mathbf{Q} = \mathrm{diag}[e^{i\mathbf{Q}_s(2s_x, 2s_y, 0)}], \quad \mathbf{P} = \mathrm{diag}[e^{i\gamma_p h}], \tag{31}$$

and where $s_x = s_y = D/2$.

Suppose a stack of s pairs of crossed gratings is characterized by reflection and transmission matrices $\mathcal{R}_a^s$ and $\mathcal{T}_a^s$ for incidence from above the structure and corresponding matrices $\mathcal{R}_b^s$ and $\mathcal{T}_b^s$ for incidence from below. To this stack, we add another pair of crossed gratings, characterized by the reflection and transmission matrices $\mathcal{R}_a$, $\mathcal{T}_a$, $\mathcal{R}_b$, and $\mathcal{T}_b$. Using a similar procedure to that described in Sec. III A, we find that the resulting structure of $s+1$ pairs has reflection and transmission matrices given by

$$\mathcal{R}_a^{s+1} = \mathcal{R}_a + \mathcal{T}_b \mathcal{R}_a^s (\mathcal{I} - \mathcal{R}_b \mathcal{R}_a^s)^{-1} \mathcal{T}_a, \tag{32}$$

$$\mathcal{T}_a^{s+1} = \mathcal{T}_a^s (\mathcal{I} - \mathcal{R}_b \mathcal{R}_a^s)^{-1} \mathcal{T}_a, \tag{33}$$

$$\mathcal{R}_b^{s+1} = \mathcal{R}_b^s + \mathcal{T}_a^s \mathcal{R}_b (\mathcal{I} - \mathcal{R}_a^s \mathcal{R}_b)^{-1} \mathcal{T}_b^s, \tag{34}$$

$$\mathcal{T}_b^{s+1} = \mathcal{T}_b (\mathcal{I} - \mathcal{R}_a^s \mathcal{R}_b)^{-1} \mathcal{T}_b^s. \tag{35}$$

IV. BAND STRUCTURE

The woodpile photonic crystal is a semi-infinite structure, with surface layers and a bulk structure. Here we concentrate on the bulk structure, which may be regarded as having a body-centered tetragonal (bct) lattice symmetry [5], together with a basis consisting of a pair of crossed rods. Each pair of crossed gratings gives a single planar layer of lattice points. The primitive lattice vectors of this 2D layer are $\mathbf{a}_1 = 2s_x \mathbf{e}_x$ and $\mathbf{a}_2 = 2s_y \mathbf{e}_y$, where $s_x = s_y = D/2$. Stacking of pairs of crossed gratings is done by means of the primitive translation vector $\mathbf{a}_3 = s_x \mathbf{e}_x + s_y \mathbf{e}_y + s_z \mathbf{e}_z$, where $s_z = 2h$.

The vectors $\mathbf{b}_1 = \pi \mathbf{e}_x / s_x$ and $\mathbf{b}_2 = \pi \mathbf{e}_y / s_y$ are the 2D reciprocal lattice vectors corresponding to the 2D lattice vectors $\mathbf{a}_1$ and $\mathbf{a}_2$. The Wigner-Seitz cell associated with this 2D reciprocal lattice structure is the surface Brillouin zone [11] and has the full symmetry of a single grating layer. Define

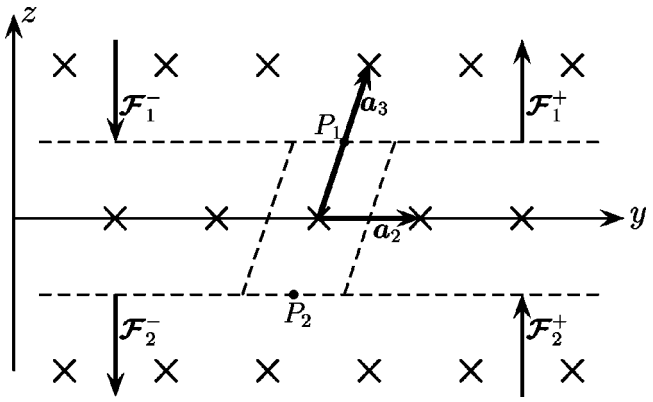

FIG. 3. Projection of the geometry of the unit cell onto the y-z plane. The crosses denote lattice points, where the middle layer is displaced into the plane of the page by a distance $D/2$.

$\mathbf{b}_3 = 2\pi \mathbf{e}_z / s_z$ and define a 3D reduced $\mathbf{k}$ zone V_r^* by

$$V_r^* = \{\mathbf{k} = k_x \mathbf{b}_1 + k_y \mathbf{b}_2 + k_z \mathbf{b}_3 \in \mathbb{R}^3\}, \tag{36}$$

where $k_x \in [0, \pi/s_x]$, $k_y \in [0, k_x]$, and $k_z \in [0, \pi/s_z]$. It is easy to see that this reduced $\mathbf{k}$ zone is completely equivalent to the usual Brillouin zone for the structure in the sense that if P is a point in one of these zones, then either P will also be in the other zone or differ from some point Q in the other zone by a reciprocal lattice vector.

We remark that the woodpile may also be considered as a face-centered tetragonal (fct) lattice symmetry with lattice vectors $\mathbf{e}_1 = 2s_x \mathbf{e}_x$, $\mathbf{e}_2 = s_x \mathbf{e}_x + s_y \mathbf{e}_y + s_z \mathbf{e}_z$, and $\mathbf{e}_3 = s_x \mathbf{e}_x - s_y \mathbf{e}_y + s_z \mathbf{e}_z$. In the special case $D/h = 2\sqrt{2}$, that is $s_z/s_x = \sqrt{2}$, the lattice is face-centered cubic (fcc). However, the bct aspect is more suited to our formulation.

Crucial to the characterization of field propagation in the bulk of the woodpile is the elaboration of its eigenstates or Bloch modes, which form a complete basis in which to expand all field terms [26]. These modes are derived via plane wave representations of the field immediately above and below any layer [1,25]

In the nomenclature of Sec. II, we denote fields incident from above and below a grating layer by partitioned vectors of plane wave coefficients $\mathcal{F}_I^{\mp}$ and outgoing fields by partitioned vectors $\mathcal{F}_D^{\pm}$ [Eq. (5)]. In this section, our basic unit is a pair of crossed cylindrical gratings, comprising a single planar layer of lattice points. It is convenient to write $\mathcal{F}_1^-$ and $\mathcal{F}_2^+$, respectively, for the incoming fields above and below the layer, where these fields are now referred to the phase origins at P_1 and P_2 (Fig. 3). The outgoing fields $\mathcal{F}_1^+$ (above the layer) and $\mathcal{F}_2^-$ (below the layer) are expressed in terms of the interaction of the incident fields with the basic layer through the equations

$$\mathcal{F}_1^+ = \mathcal{R}_a \mathcal{F}_1^- + \mathcal{T}_b \mathcal{F}_2^+, \tag{37}$$

$$\mathcal{F}_2^- = \mathcal{T}_a \mathcal{F}_1^- + \mathcal{R}_b \mathcal{F}_2^+. \tag{38}$$

The Bloch condition for field quasiperiodicity in the direction $\mathbf{a}_3$ imposes the constraint

$$\mathcal{F}_2^{\pm} = \mu \mathcal{F}_1^{\pm} \quad \text{with} \quad \mu = \exp(-i\mathbf{k}_0 \cdot \mathbf{a}_3), \tag{39}$$

where $\mathbf{k}_0$ denotes the Bloch vector, and, following Ref. [25], this constraint may be formulated as the eigenvalue problem

$$\mathsf{T}\begin{bmatrix} \mathcal{F}_1^- \\ \mathcal{F}_1^+ \end{bmatrix} = \mu \begin{bmatrix} \mathcal{F}_1^- \\ \mathcal{F}_1^+ \end{bmatrix}, \tag{40}$$

in which

$$\mathsf{T} = \begin{bmatrix} \mathcal{T}_a - \mathcal{R}_b \mathcal{T}_b^{-1} \mathcal{R}_a & \mathcal{R}_b \mathcal{T}_b^{-1} \\ -\mathcal{T}_b^{-1} \mathcal{R}_a & \mathcal{T}_b^{-1} \end{bmatrix} \tag{41}$$

is the interlayer translation operator.

The modes of the crystal are the eigenstates of the matrix operator T and we must solve Eq. (40) where μ is the eigenvalue (or Bloch factor) and the corresponding eigenstates define the modes, which, at the interlayer boundaries, are given by plane wave expansions referred to above. When dealing with exact, untruncated field representations, only a finite number of the modes are propagating states, that is for them $|\mu|=1$ (which can only occur in lossless systems), while an unbounded number are evanescent with $|\mu|<1$ or $|\mu|>1$. In practice, the field expansions must be truncated for computational purposes, thus leading to the solution of a finite-dimensional algebraic eigenvalue problem. It is the propagating states $\mu = e^{-i\mathbf{k}_0 \cdot \mathbf{a}_3}$ that are of greatest interest. Their importance lies in their capacity to carry energy over arbitrary distances within the crystal. Band gaps are characterized by the complete absence of propagating states, thus removing the mechanism of energy transmission through the crystal. All of the states are then evanescent, which leads to fields decaying in one direction or the other. As we shall show, this decay is given asymptotically by a power law $|\mu|^{\ell}$, where ℓ is the number of layers traversed by the mode and μ is the eigenvalue of the dominant mode.

The method outlined above involving the matrix T is theoretically exact, but of limited practical use, due to numerical instabilities which arise in the inversion of the transmission scattering matrices, necessary for the evaluation of T. The calculation of eigenvalues and eigenvectors from Eq. (40) thus suffers from ill conditioning that causes catastrophic numerical errors with increasing matrix dimension. These errors manifest themselves particularly in the case of 3D problems, such as the woodpile, for which the plane wave orders are doubly dimensioned. These problems may be avoided by an alternative formulation (the R matrix formulation), details of which are given in Refs. [1,19].

In Fig. 4, we show a projected band diagram of an infinite woodpile. The vertical axis is proportional to the wavenumber, while the horizontal axis traverses the irreducible part of the projected Brillouin zone, shown in the inset to the figure. For the woodpile, the projected Brillouin zone is a square and, from symmetry arguments, one need consider only the irreducible octant labeled ΓXM in Fig. 4. Each point on the perimeter of the path thus determines an (α_0, β_0) pair for which we solve the eigenvalue problem to yield k_{0z}. The density of shading in the diagram is in direct proportion to the number of propagating states for this (α_0, β_0) pair, with the white region corresponding to the absence of any propagating states. Clearly evident is a range of frequencies for which there are no propagating states. This feature is a complete band gap, in which propagation at all such frequencies and in all possible directions is suppressed. It is the presence of these complete band gaps that enables the flow of light to be precisely controlled and guided, through the introduction of defects into the lattice.

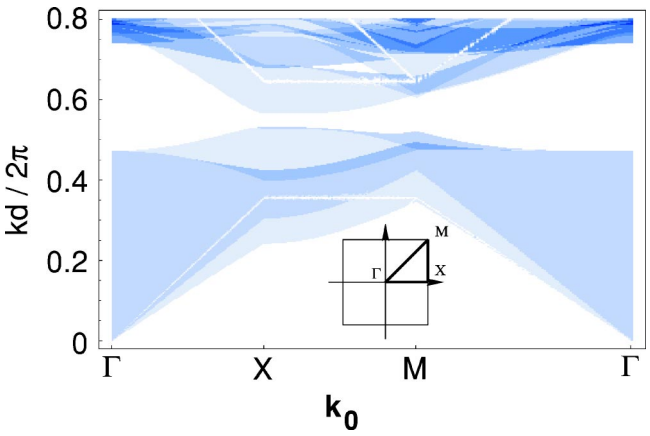

FIG. 4. (Color online) Two-dimensional projection of the band structure of an infinite dielectric woodpile crystal. The cylindrical rods have radii of 0.1 μm and refractive index 3.6, the pitch D is 0.711 μm, and the separation h between layers is 0.21 μm.

The effect of the number of layers

As discussed in Refs. [1,25], the eigenvalues are divided into forward and backward propagating states, with each forward state paired with a backward state. For evanescent states, which carry no energy, those with eigenvalue $|\mu|<1$ are regarded as forward propagating, while those with $|\mu|>1$ are regarded as backward propagating.

For states which carry energy, the treatment is more delicate, requiring a calculation of the downgoing flux E_F. Those states with $E_F>0$ are regarded as forward propagating, while those with $E_F<0$ are backward propagating [1,25].

With all modes partitioned as above, we recast Eq. (40) in the form

$$\mathsf{T}\tilde{\mathsf{F}} = \tilde{\mathsf{F}}\tilde{\mathbf{\Lambda}}, \tag{42}$$

where

$$\tilde{\mathsf{F}} = \begin{bmatrix} \mathsf{F}_- \mathsf{F}'_- \\ \mathsf{F}_+ \mathsf{F}'_+ \end{bmatrix} \quad \text{and} \quad \tilde{\mathbf{\Lambda}} = \begin{bmatrix} \mathbf{\Lambda} & \mathbf{0} \\ \mathbf{0} & \mathbf{\Lambda}' \end{bmatrix}. \tag{43}$$

The left and right partitions of the block structured matrix $\tilde{\mathsf{F}}$ and the diagonal matrices $\mathbf{\Lambda} = \mathrm{diag}[\mu_i]$ and $\mathbf{\Lambda}' = \mathrm{diag}[\mu'_i]$ that constitute the left and right partitions of $\tilde{\mathbf{\Lambda}}$ correspond, respectively, to the forward and backward propagation problems. Here $|\mu_i| \leqslant 1$ and $|\mu'_i| \geqslant 1$.

Now consider a 2ℓ layer structure consisting of ℓ crossed pairs of gratings. At the nth pair $(0 \leqslant n \leqslant \ell)$ the field may be written as a linear combination of eigenstates:

$$\begin{bmatrix} \mathcal{F}^- \\ \mathcal{F}^+ \end{bmatrix} = \begin{bmatrix} \mathsf{F}_- \mathsf{F}'_- \\ \mathsf{F}_+ \mathsf{F}'_+ \end{bmatrix} \begin{bmatrix} \mathbf{\Lambda}^n & \mathbf{0} \\ \mathbf{0} & (\mathbf{\Lambda}')^{-(\ell-n)} \end{bmatrix} \begin{bmatrix} \mathbf{C}_- \\ \mathbf{C}_+ \end{bmatrix}, \tag{44}$$

for constant vectors $\mathbf{C}_-$ and $\mathbf{C}_+$. We denote the incident field from above by $\boldsymbol{\delta}$, the reflected field at the surface by $\mathbf{r}_\ell$, and the transmitted field at the bottom of the structure by $\mathbf{t}_\ell$.

Then, putting $n=0$ in Eq. (44), we have

$$\begin{bmatrix} \boldsymbol{\delta} \\ \mathbf{r}_\ell \end{bmatrix} = \begin{bmatrix} \mathsf{F}_- \\ \mathsf{F}_+ \end{bmatrix} \mathbf{C}_- + \begin{bmatrix} \mathsf{F}'_- \\ \mathsf{F}'_+ \end{bmatrix} (\mathbf{\Lambda}')^{-\ell} \mathbf{C}_+ . \tag{45}$$

Similarly, putting $n=\ell$ in Eq. (44) yields

$$\begin{bmatrix} \mathbf{t}_\ell \\ \mathbf{0} \end{bmatrix} = \begin{bmatrix} \mathsf{F}_- \\ \mathsf{F}_+ \end{bmatrix} \mathbf{\Lambda}^n \mathbf{C}_- + \begin{bmatrix} \mathsf{F}'_- \\ \mathsf{F}'_+ \end{bmatrix} \mathbf{C}_+ , \tag{46}$$

assuming that there is no incident field from below the structure. After some matrix manipulation, we find that

$$\mathbf{r}_\ell = [\mathcal{R} - (\mathcal{P}')^\ell \mathcal{R} \mathcal{P}^\ell][\mathcal{I} - \mathcal{R}'(\mathcal{P}')^\ell \mathcal{R} \mathcal{P}^\ell]^{-1} \boldsymbol{\delta}, \tag{47}$$

$$\mathbf{t}_\ell = (\mathcal{I} - \mathcal{R}'\mathcal{R}) \mathcal{P}^\ell [\mathcal{I} - \mathcal{R}'(\mathcal{P}')^\ell \mathcal{R} \mathcal{P}^\ell]^{-1} \boldsymbol{\delta}, \tag{48}$$

where

$$\mathcal{R} = \mathsf{F}_+ \mathsf{F}_-^{-1}, \quad \mathcal{P} = \mathsf{F}_- \mathbf{\Lambda} \mathsf{F}_-^{-1}, \tag{49}$$

$$\mathcal{R}' = \mathsf{F}'_- (\mathsf{F}'_+)^{-1}, \quad \mathcal{P}' = \mathsf{F}'_+ (\mathbf{\Lambda}')^{-1} (\mathsf{F}')_+^{-1} . \tag{50}$$

In a band gap, $(\mathcal{P}')^\ell \to \mathbf{0}$ as $\ell \to \infty$, so

$$\mathbf{t}_\ell = (\mathsf{F}_- - \mathcal{R}'_- \mathsf{F}_+) \mathbf{\Lambda}^\ell (\mathsf{F}_-^{-1} \boldsymbol{\delta}), \tag{51}$$

which shows explicitly that the asymptotic behavior of the transmittance with increasing ℓ is governed by its dominant eigenvalue and that the field intensity decays as $|\mu|^{2\ell}$ within a band gap.

For a semi-infinite structure with each layer having an arbitrarily small amount of loss, we have $\mathbf{t}_\infty = 0$, while for all structures, whether lossy or not [24],

$$\mathbf{r}_\infty = \mathsf{F}_+ \mathsf{F}_-^{-1} \boldsymbol{\delta} = \mathsf{R}_\infty \boldsymbol{\delta}, \tag{52}$$

where $\mathsf{R}_\infty = \mathsf{F}_+ \mathsf{F}_-^{-1}$ is the scattering matrix for an infinite woodpile.

V. METALLIC GRATINGS

Recently, metallic photonic crystals have been fabricated at Sandia Laboratories [9]. However, investigation of their photonic band gap properties, especially in the infrared and visible spectrum can be challenging because metals are strongly dispersive and absorbing in these regions. A strong advantage of the multipole theory we have developed is that it is able to accommodate metallic gratings without difficulty.

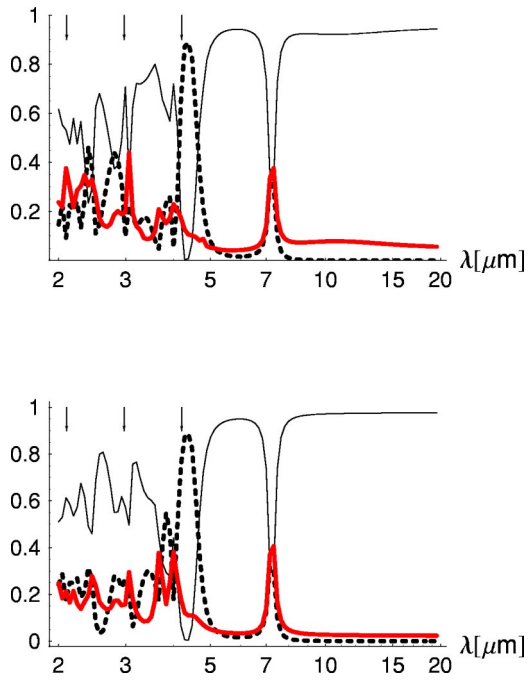

FIG. 5. (Color online) Four layer woodpile, showing absorptance, reflectance, and transmittance (thick, thin, and dashed curves, respectively) as a function of wavelength λ. The incidence is vertical, with the electric field perpendicular to the top layer of rods (above) and parallel to it (below). The rod diameters are 1.6 μm, the pitch is 4.2 μm, and the center-to-center layer spacing is 1.7 μm. The arrows show the Rayleigh wavelengths.

This is because our input parameters are all frequency dependent, so in order to model phenomena over a range of frequencies, we need only loop over all frequencies, while changing the input data (such as complex refractive index) for each new frequency. We have modeled grids composed of tungsten, for which the frequency-dependent refractive index is taken from Palik [21]. This enters into our formulation via the matrix $\mathcal{M}$, introduced in Sec. II.

The photonic crystals that have been fabricated at Sandia Laboratories [9] are tungsten woodpile structures consisting of rectangular rods, with a filling fraction of 28%. In Ref. [9], comparisons were made between experiment and theory for unpolarized incident radiation and some differences were evident. For comparison purposes, we have modeled a structure consisting of circular rods also with a filling fraction of 28% (Fig. 5). As distinct from the results in Ref. [9], we show results for normally incident radiation for both polarizations of the incident beam. This is of interest since the surface structure of the woodpile is not polarization insensitive, even though its bulk structure is. One interesting feature of Fig. 5 is that the reflectance, transmittance, and absorptance of the four layer woodpile agree well for both polarizations for wavelengths longer than the grid period. At very long wavelengths, that for the $H_\parallel$ case where the magnetic field is oriented parallel to the rods in the top layer, there is a lower reflectance than the orthogonal $E_\parallel$ polarization. This is easily understood on the basis of average dielectric constant: for $H_\parallel$ we average the inverse dielectric constant [27], giving a lower result than for $E_\parallel$ polarization, where the normal

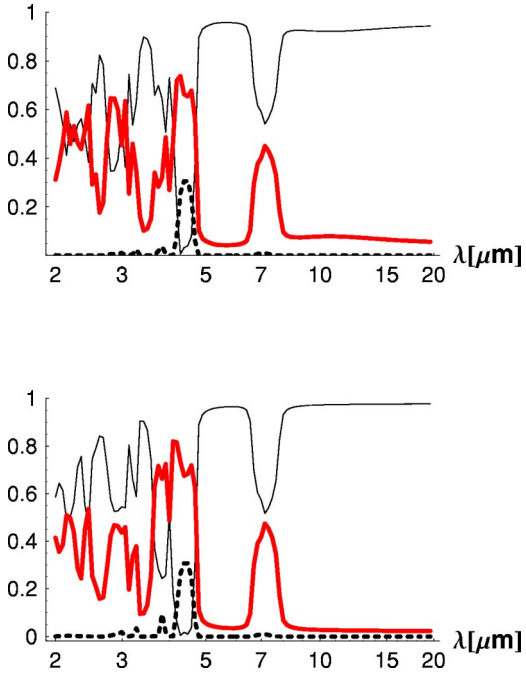

FIG. 6. (Color online) As Fig. 5, but for 40 layers.

average of dielectric constant is calculated. For both the polarizations, there is a narrow plasmon absorption peak near 7 μm, causing a drop in reflectance there. A second, more pronounced drop in reflectance occurs at the first Rayleigh wavelength of the woodpile $\lambda = D$. At shorter wavelengths, there are significant differences in the reflectance, transmittance, and absorptance for the two polarizations. The $H_{\|}$ curve exhibits a more ragged variation of reflectance with wavelength, in keeping with previous work on diffraction anomalies in metallic inductive grids [28].

The difference between surface effects and bulk effects is made more evident in Fig. 6, where we show reflectance, transmittance, and absorptance for 40 layer woodpiles. Note that the transmittance is now only appreciable in a narrow band on the long wavelength side of the first Rayleigh wavelength. Even this region of enhanced transmittance must disappear with the addition of more layers, as a consequence of the lossy nature of each layer of the woodpile. The polarization differences for wavelengths below the first Wood anomaly are similar in character for forty layers to the four layer case.

Figure 7 also shows the effect of polarization of the incident beam for a different cylinder radius from Figs. 5 and 6, and also for semi-infinite stacks. For this case, the woodpile

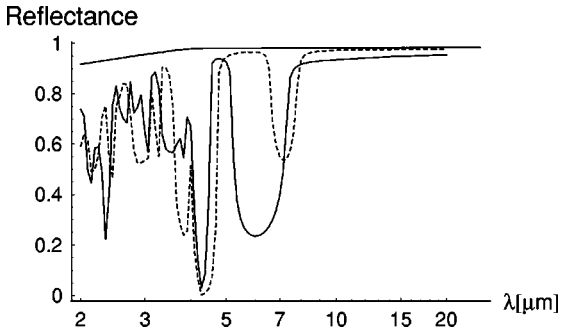

FIG. 7. Semi-infinite tungsten woodpile, showing reflectance as a function of wavelength λ (μm) for vertical incidence. The solid curve is the case where the incident electric field vector is orthogonal to the top layer of rods, while the dashed curve is the case where the incident electric field vector is parallel to the top layer of rods. The solid line at the top of the graph is the reflectance of bulk tungsten. The rod diameters are 1.2 μm, the pitch is 4.2 μm, and the center-to-center layer spacing is 1.3 μm.

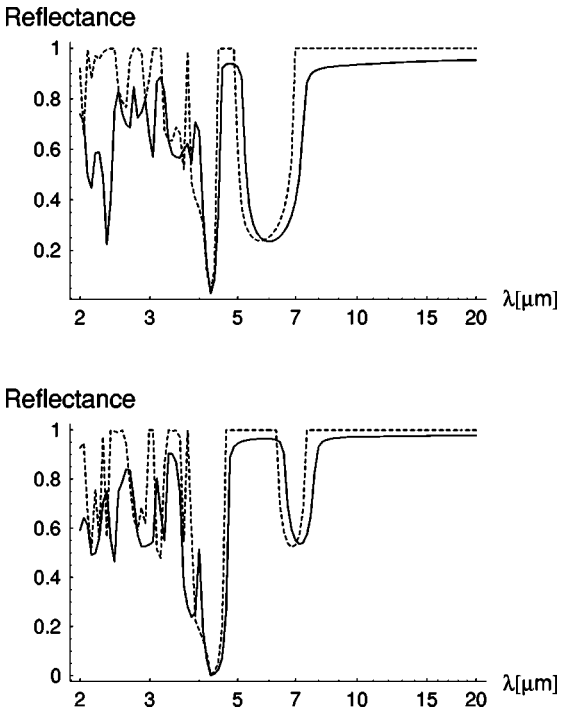

FIG. 8. Semi-infinite tungsten woodpile as in Fig. 7 compared with a perfect conductor of the same physical dimensions, showing reflectance as a function of wavelength λ (μm) for vertical incidence with the incident electric vector perpendicular to the top layer of rods (above) and parallel to it (below).

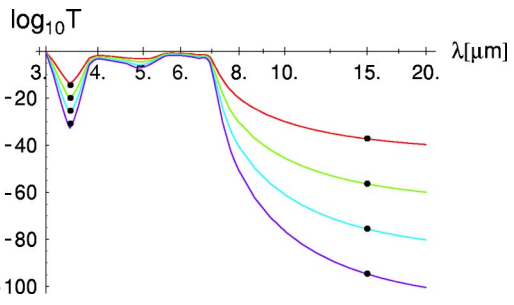

FIG. 9. (Color online) Tungsten woodpile, showing logarithm of transmittance for 20, 30, 40, 50 layers. The plotted dot points show spacings of $20\ln|\mu|$ determined by the dominant eigenvalue μ, where $|\mu| = 0.534\,549$ when $\lambda = 3.5$ and $|\mu| = 0.098\,242\,1$ when $\lambda = 15$. The rod diameters are 1.2 μm, the pitch is 4.2 μm, and the center-to-center layer spacing is 1.3 μm. The incidence is transverse magnetic and conical with wave vector in the direction of the unit vector $\hat{\mathbf{u}} = 0.358\hat{\mathbf{x}} + 0.268\hat{\mathbf{y}} + 0.894\hat{\mathbf{z}}$.

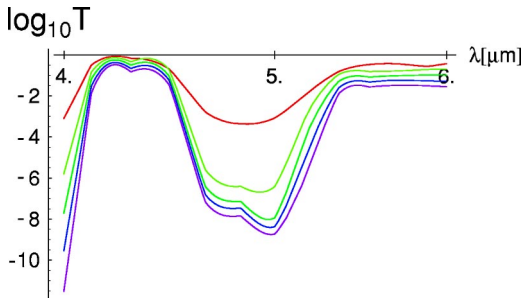

FIG. 10. (Color online) Tungsten woodpile, showing logarithm of transmittance for 10, 20, 30, 40, 50 layers as a function of wavelength λ (μm). The rod diameters are 1.2 μm, the pitch is 4.2 μm, and the center-to-center layer spacing is 1.3 μm. The incidence is vertical, with the electric field orthogonal to the top layer of rods. The nonuniform decrease in transmittance at 5 μm for each additional set of 10 layers is evident (See the text for further discussion).

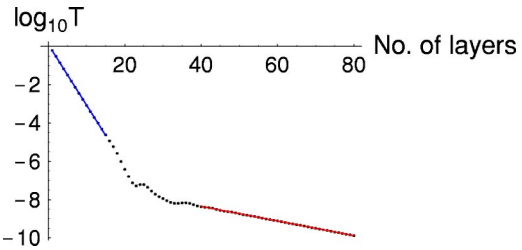

FIG. 11. (Color online) The tungsten woodpile of Fig. 10, showing logarithm of transmittance as a function of increasing layer number at a wavelength of 5 μm. The initial decay represents a Bloch mode with eigenvalue of absolute value 0.695 544 and Bloch coefficient 3.215 19, while the asymptotic decay is due to the Bloch mode with the dominant eigenvalue having absolute value 0.957 053, but with the small coefficient of 0.095 947 8.

transmittance is zero, the reflectance is calculated from Eq. (52), and the absorptance is the complement of the reflectance. Note that the plasmon absorption peaks near 7 μm differ substantially for the two polarizations, demonstrating conclusively that they manifest surface rather than bulk plasmon effects. The fact that the plasmon absorption peak for $H_{\|}$ polarization is wider and deeper than that for $E_{\|}$, again is in keeping with theoretical and experimental studies on metallic crossed gratings [28,29].

In Fig. 8 we compare tungsten woodpiles and woodpiles made of perfectly conducting cylinders. The perfect conductivity case is treated by modifying the boundary conditions that occur in the matrix $\mathcal{M}$ of Eq. (8), a further illustration of the versatility of the multipole method. The polarization effects for the perfect conductor are similar to those for tungsten. A notable feature in Fig. 8 is the difference in the width of the reflection dip near 7 μm for the two polarizations. Note that for both the polarizations the reflectance drop occurs well on the long wavelength side of the first Rayleigh wavelength, even for the infinite conductance case. As for the latter, one would expect the surface plasmon resonance for a structure with shallow modulation to coincide with the Rayleigh wavelength, this illustrates the dominant role of the woodpile geometry in determining the position of the dip.

As we showed in Sec. IV, the asymptotic behavior of the transmittance with increasing ℓ is governed by its dominant eigenvalue and that the field intensity decays as $|\mu|^{2\ell}$ within a band gap. This is clearly shown in Fig. 9, where each additional group of 10 layers causes the transmission to drop by a factor determined by the dominant eigenvalue. On the other hand, if a particular Bloch mode has a large coefficient, the initial attenuation is dominated by this mode. Only after sufficiently many layers have been added will the asymptotic attenuation become apparent. This behavior is shown in Figs. 10 and 11.

VI. CONCLUSION

In this paper, we have given a theoretical account of the woodpile photonic crystal, including the derivation of explicit analytic expressions for the reflectance, transmittance, and absorptance of a structure with either a finite or an infinite number of layers. In the case of a finite structure, we have shown how the transmittance, reflectance, and absorptance for a given number of layers depends on the eigenvalues and Bloch coefficients of the layer transfer matrix T of Eq. (41). Our treatment enables us to analyze both dielectric and metallic woodpiles, including the case of perfect conductivity, where in the metallic case we are able to use measured values of optical constants.

Our theory enables us to generate numerical results such as band diagrams of dielectric woodpiles and graphs of reflectance, transmittance, and absorptance of both dielectric and metallic woodpiles. Numerical studies have demonstrated polarization dependence for metallic woodpiles, showing that the surface layer of a woodpile crystal plays an important role in the observed effect, and emphasizing the importance of studying the polarization dependence of the optical properties of woodpiles, even for normally incident radiation.

ACKNOWLEDGMENT

The support of the Australian Research Council for the Center of Excellence for Ultra-high-bandwidth Devices for Optical Systems (CUDOS) is acknowledged.

[1] G.H. Smith, L.C. Botten, R.C. McPhedran, and N.A. Nicorovici, Phys. Rev. E **66**, 056604 (2002).
[2] J.P. Dowling, http://home.earthlink.net/~jpdowling/pbgbib.html
[3] K.M. Ho, C.T. Chan, C.M. Soukoulis, R. Biswas, and M.M. Sigalas, Solid State Commun. **89**, 413 (1994).
[4] E. Özbay, A. Abeyta, G. Tuttle, M. Tringides, R. Biswas, C.T. Chan, C.M. Soukoulis, and K.M. Ho, Phys. Rev. B **50**, 1945

(1994).
[5] H.S. Sözüer and J.P. Dowling, J. Mod. Opt. **41**, 231 (1994).
[6] S.Y. Lin and J.G. Fleming, IEEE Journal of Lightwave Technology **17**, 1944 (1999).
[7] S.Y. Lin and J.G. Fleming, Opt. Lett. **24**, 49 (1999).
[8] S. Noda, K. Tomoda, N. Yamamoto, and A. Chutinan, Science (Washington, D.C., U.S.) **289**, 604 (2000).
[9] J.G. Fleming, S.Y. Lin, I. El-Kady, and K.M. Ho, Nature (London) **417**, 52 (2002).
[10] I. El-Kady, M.M. Sigalas, R. Biswas, K.M. Ho, and C.M. Soukoulis, Phys. Rev. B **62**, 15299 (2000).
[11] A. Modinos, N. Stefanou, and V. Yannopapas, Opt. Express **8**, 197 (2001).
[12] R.C. McPhedran, L.C. Botten, A.A. Asatryan, N.A. Nicorovici, P.A. Robinson, and C.M. de Sterke, Phys. Rev. E **60**, 7614 (1999).
[13] L.C. Botten, N.A. Nicorovici, A.A. Asatryan, R.C. McPhedran, C.M. de Sterke, and P.A. Robinson, J. Opt. Soc. Am. A **17**, 2165 (2000).
[14] L. Li, J. Mod. Opt. **40**, 553 (1993).
[15] L.C. Botten, M.S. Craig, R.C. McPhedran, J.L. Adams, and J.R. Anderwartha, Opt. Acta **28**, 413 (1981).
[16] E. Centeno and D. Felbacq, J. Opt. Soc. Am. **17**, 320 (2000).
[17] D. Felbacq and E. Centeno, Opt. Commun. **199**, 39 (2001).
[18] B. Gralak, Ph.D. thesis, Université Aix-Marseille, 2001.
[19] B. Gralak, S. Enoch, and G. Tayeb, J. Opt. Soc. Am. A **19**, 1547 (2002).
[20] R.C. McPhedran, L.C. Botten, A.A. Asatryan, N.A. Nicorovici, C.M. de Sterke, and P.A. Robinson, Aust. J. Phys. **52**, 791 (1999).
[21] E.D. Palik, *The Handbook of Optical Constants of Solids* (Academic, New York, 1993).
[22] R.C. McPhedran, N.A. Nicorovici, L.C. Botten, and K.-D. Bao, *Green's Function, Lattice Sums and Rayleigh's Identity for a Dynamic Scattering Problem*, IMA Volumes in Mathematics and its Applications Vol. 96 (Springer-Verlag, New York, 1997), pp. 155–186.
[23] N.A. Nicorovici and R.C. McPhedran, Phys. Rev. E **50**, 3143 (1994).
[24] L.C. Botten, N.A. Nicorovici, A.A. Asatryan, R.C. McPhedran, C.M. de Sterke, and P.A. Robinson, J. Opt. Soc. Am. A **17**, 2177 (2000).
[25] L.C. Botten, N.A. Nicorovici, R.C. McPhedran, C.M. de Sterke, and A.A. Asatryan, Phys. Rev. E **64**, 046603 (2001).
[26] G. Allaire, C. Conca, and M. Vanninathan, in Actes du 29ème Congrès d'Analyse Numérique, ESAIM Proceedings, 1998 (unpublished), Vol. 3, pp. 65–84.
[27] G. Milton, *The Theory of Composites*, Cambridge Monographs on Applied and Computational Mathematics, Vol. 6 (Cambridge University Press, Cambridge, 2002).
[28] *Electromagnetic Theory of Gratings*, edited by R. Petit, Topics in Current Physics Vol. 22 (Springer-Verlag, Berlin, 1980).
[29] R.C. McPhedran, N.A. Nicorovici, L.C. Botten, C.M. de Sterke, P.A. Robinson, and A.A. Asatryan, Opt. Commun. **168**, 47 (1999).